Multiple scattering from assemblies of dislocation walls in three dimensions. Application to propagation in polycrystals

Agnès Maurel[a)]
Laboratoire Ondes et Acoustique, UMR CNRS 7587, Ecole Supérieure de Physique et de Chimie Industrielles, 10 rue Vauquelin, 75005 Paris, France

Vincent Pagneux
Laboratoire d'Acoustique de l'Université du Maine, UMR CNRS 6613 Av. Olivier Messiaen, 72085 Le Mans Cedex 9, France.

Felipe Barra and Fernando Lund
Departamento de Física, Facultad de Ciencias Físicas y Matemáticas, Universidad de Chile, Casilla 487–3, Santiago, Chile and Centro para la Investigación Interdisciplinaria Avanzada en Ciencias de los Materiales (CIMAT), Universidad de Chile, Santiago, Chile

(Received 20 June 2006; revised 21 March 2007; accepted 30 March 2007)

The attenuation of ultrasound in polycrystalline materials is modeled with grain boundaries considered as arrays of dislocation segments, a model valid for low angle mismatches. The polycrystal is thus studied as a continuous medium containing many dislocation "walls" of finite size randomly placed and oriented. Wave attenuation is blamed on the scattering by such objects, an effect that is studied using a multiple scattering formalism. This scattering also renormalizes the speed of sound, an effect that is also calculated. At low frequencies, meaning wavelengths that are long compared to grain boundary size, then attenuation is found to scale with frequency following a law that is a linear combination of quadratic and quartic terms, in agreement with the results of recent experiments performed in copper [Zhang *et al.*, J. Acoust. Soc. Am. **116**(1), 109–116 (2004)]. The prefactor of the quartic term can be obtained with reasonable values for the material under study, without adjustable parameters. The prefactor of the quadratic term can be fit assuming that the drag on the dynamics of the dislocations making up the wall is one to two orders of magnitude smaller than the value usually accepted for isolated dislocations. The quartic contribution is compared with the effect of the changes in the elastic constants from grain to grain that is usually considered as the source of attenuation in polycrystals. A complete model should include this scattering as well. © *2007 Acoustical Society of America.* [DOI: 10.1121/1.2734488]

PACS number(s): 43.35.Cg, 43.20.Hq, 43.20.Fn [RLW] Pages: 3418–3431

I. INTRODUCTION

Ultrasonic materials characterization and nondestructive evaluation need the scattering of elastic waves in polycrystalline materials to be precisely understood since ultrasonic attenuation and backscatter measurements are used widely to extract the microstructural parameters such as grain size and also to detect flaws in materials.

Most of the current understanding of the acoustic attenuation in polycrystals is due to models that consider the wave scattering caused by the variations of the elastic properties from one grain to the other that result from the different orientations of the single crystals. Grain boundaries are, at least implicitly, treated as structureless, as well as passive, surfaces. Pioneer works from the 1940s to the 1960s[1–4] predicted a quartic dependence of the attenuation on the frequency (Rayleigh scattering) in the low frequency regime. Further refinements have been considered, mainly to include the texture or anisotropy of materials[5–10] (see also the review in Ref. 11) all producing the Rayleigh scattering solution at low frequencies.

Recent improvements in sample preparation and in measurement methods have allowed the comparison, on a quantitative basis, of experimental results with theoretical models. Zhang *et al.*[12] performed accurate measurements of ultrasound attenuation in copper and copper-aluminum samples; they were able to establish a frequency dependence of the attenuation as a combination of quadratic and quartic terms, a behavior that is not explained by current theoretical models. Let us also mention the recent work of Hurley *et al.*[13] where the refraction of surface acoustic waves across a single grain boundary has been visualized and measured using optical techniques.

In a previous paper,[14] we have proposed a model that focuses on the grain boundaries as the source of scattering. This was done by modeling grain boundaries as dislocation arrays in two dimensions. In the present study, we generalize the study to three-dimensional configurations: the grains are assumed to be limited by "walls" formed of arrays of dislocations, as pictured in Fig. 1. We expect that scattering by such dislocation walls can produce the combination of quadratic and quartic frequency terms for the attenuation in the low frequency regime, as we have observed this behavior for randomly distributed dislocation segments.[15]

[a)]Electronic mail: agnes.maurel@ espci.fr

 0001-4966/2007/121(6)/3418/14/$23.00

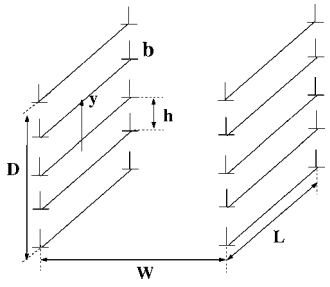

FIG. 1. Schematic representation of two low-angle grain boundaries of size $L \times D$ separated by a distance w. The dislocation segment holds edge dislocations, with Burgers vector b, separated by a distance h.

Since Burgers[16] and Bragg[17] in 1940, low angle grain boundaries are known to be described by arrays of edge dislocations. In the 1950s, the works of Shockley and Read[18,19] showed that the grain boundary energy can be expressed as the energy of a suitable periodic array of dislocations with dislocation spacing h expressed as a function of Burgers vector b and of the misorientation θ between two grains in the so-called Frank formula $b=2h \sin \theta/2$.[20] The validity of this model appears to be well established for typical dislocation spacings larger than about four interatomic distances.[21,22]

There does not appear the same degree of consensus concerning the structure of high angle grain boundaries, for whose modeling different approaches have been proposed. Most of them belong to, or are derived from, the coincident site lattice model, from the O-lattice model or from dislocation theories[23–26] (see also the review in Ref. 27, and references herein) and they are based on a geometrical analysis of the crystallography of the boundary. The experimental works on grain boundary structure[28–33] contribute to that kind of analysis. Let us also mention the work of Kobayashi *et al.*[34] that analyzes the energy of a grain boundary in a continuum model and the work of Meilikhov,[35] who recovered superconductive features of grain boundaries using a model of edge dislocations randomly distributed on the boundary, instead of regularly spaced.

The main simplification of this paper is to consider a polycrystal endowed only with low angle grain boundaries, pictured as walls holding dislocations distributed in both directions of the walls. The distribution law of the dislocation lines on the grain boundaries is discussed in the paper, either periodic or random, discrete or continuous. Otherwise, the elastic properties of the grains are isotropic and homogeneous. Thus, the only source of scattering is the presence of dislocation lines.

The paper is organized as follows: In Sec. II, we present the basic relations that allow one to treat the problem of scattering by a dislocation wall of finite size $L \times D$ that is the picture of a grain boundary. This is accomplished using a wave equation with a source term that encapsulates the wave-grain boundary interaction. The formalism of multiple scattering using the Dyson equation is applied to this differential equation and calculations, for low scattering strength, up to second order are given. This leads to a derivation of the velocity change and attenuation of both longitudinal and transverse waves, the results of which are presented in Sec. III. One important aspect of the present study is that we find a frequency dependence of acoustic attenuation that is a linear combination of quadratic and quartic terms, in agreement with the results of Zhang *et al.*[12] A more detailed comparison with those experiments is presented and discussed in Sec. IV. The quartic contribution found in our model is also compared with the quartic contribution usually found when considering the changes in elastic constants from grain to grain. Including this effect in a complete model is easy since both effects simply superimpose, as shown in Appendix C. Concluding remarks are given in Sec. VI, and technical details are given in the appendices.

II. PROPAGATION OF WAVE THROUGH A RANDOM DISTRIBUTION OF GRAIN BOUNDARIES

In this section, we present the derivation of the wave numbers for coherent waves propagating in an effective medium that is an elastic medium filled with a random distribution of dislocation walls of finite size. This is our picture of the grain boundaries. It does not consider their actual topology, an effect that should not be important at long wavelengths. These wave numbers have a real part, which differs from the real wave numbers $\omega/c_{L,T}$ in the absence of grain boundaries, and an imaginary part, corresponding to the attenuation of the propagating waves.

The derivation is performed using a usual multiple scattering theory, solving the Dyson equation assuming low scattering strength. This approach has been previously developed for isolated dislocation segments in Ref. 15.

In the paper, we denote (λ, μ) the Lame's coefficients and ρ the density of the elastic medium that composes the grains. With an isotropic medium, we use $c_{ijkl}=\lambda \delta_{ij}\delta_{kl} + \mu(\delta_{ik}\delta_{jl}+\delta_{il}\delta_{jk})$. With ω the angular frequency of the incident wave, the velocities of the transverse and longitudinal waves are $c_L=\sqrt{(\lambda+2\mu)/\rho}$ and $c_T=\sqrt{\mu/\rho}(\gamma \equiv c_L/c_T)$.

A. Derivation of a wave equation with a source ("potential") term

It has been shown in previous paper[36,37] that the interaction of a single moving edge dislocation with elastic waves is described by a wave equation with a source term. To do that, we described the two step scattering mechanism as pictured in Fig 2.

First, the wave incident on the dislocation segment (pinned at both extremities) induces it to oscillate. Low accelerations are also assumed, so that the backreaction of the radiation on the dislocation dynamics can be neglected. Following Ref. 38 and under these hypotheses, the equation of motion of an edge dislocation takes the form of the equation of motion for a string endowed with mass and line tension, forced by the usual Peach-Koehler force[39,40]

$$m\ddot{X}_k(s,t) + B\dot{X}_k(s,t) - \Gamma X_k''(s,t) = F_k(t), \tag{2.1}$$

and the associated boundary conditions at pinned ends $X_k(\pm L/2,t)=0$. In Eq. (2.1), $m \simeq \rho b^2$ defines a mass per unit length, $\Gamma \simeq \rho b^2 c_T^2$ a line tension, B is the drag coefficient, and $F_k=\epsilon_{kjm}\tau_m b_i \sigma_{ij}$ the Peach–Koehler force (ϵ_{ijk} denotes the usual completely antisymmetric tensor). The dislocation is assumed to be a gliding edge dislocation, so that the motion

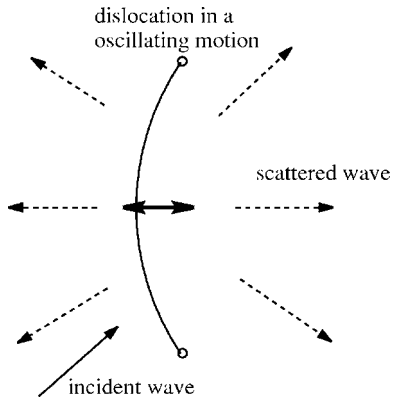

FIG. 2. Two step scattering mechanism of an elastic wave by a dislocation segment. The incident wave hits the dislocation, causing it to oscillate in response; the oscillation motion generates an outgoing scattered wave.

X occurs along the direction of the Burgers vector. We denote **t** this direction, with $\mathbf{b}=b\mathbf{t}$, $\boldsymbol{\tau}$ the direction along the dislocation line, and $\mathbf{n}\equiv\boldsymbol{\tau}\times\mathbf{t}$.

In previous papers[15,37] where interest was in the low frequency regime, this equation was solved in the limit $kL \ll 1$, so that all the points of the segment received a wave with the same phase. Here, we choose to treat the general case and the solution is

$$\dot{X}(\sigma,y,\omega) = -\frac{2}{L}\frac{\mu b}{m}\mathsf{M}_{lk}\sum_n \left\langle \frac{\partial}{\partial x_l} v_k[\mathbf{X}(\sigma',y),\omega] \middle| \chi_n(\sigma') \right\rangle \times p_n(\omega)\chi_n(\sigma) \tag{2.2}$$

with $p_n(\omega)\equiv 1/(\omega^2-n^2\omega_1^2+i\omega B/m)$, $\omega_1\equiv\pi c_T/L$, $\mathsf{M}_{lk}\equiv t_l n_k + t_k n_l$, $\chi_n(\sigma)\equiv\sin[(n\pi/L)(\sigma+L/2)]$ and where $\langle a|b\rangle \equiv \int_{-L/2}^{L/2} ab$ denotes an inner product.

In the second step, the moving dislocation emits a scattered wave whose form can be derived using the wave equation and the discontinuity relation $[\mathbf{u}]=\mathbf{b}$, first given in Ref. 41, see also Ref. 14,

$$v_m^s(\mathbf{x},t) = \epsilon_{jnh}c_{ijkl}\int_{-D/2}^{D/2} dy\, p(y)\int_{-L/2}^{L/2} d\sigma dt'\, b_i\dot{X}_n(\sigma,y,t') \times \tau_h\frac{\partial}{\partial x_l}G_{km}^0[\mathbf{x}-\mathbf{X}(\sigma,y),t-t'], \tag{2.3}$$

where the Green tensor of free space G^0 verifies

$$\rho\frac{\partial^2}{\partial t^2}G_{im}^0(\mathbf{x},t) - c_{ijkl}\frac{\partial^2}{\partial x_j\,\partial x_l}G_{km}^0(\mathbf{x},t) = \delta(\mathbf{x})\,\delta(t)\,\delta_{im}. \tag{2.4}$$

In Eq. (2.4), $p(y)$ describes the distribution of the dislocation lines along the grain boundary of length D (along the y axis), with $\int dy\, p(y)=N$ the number of elementary dislocation lines held by the grain boundary.

A number of possibilities are open for $p(y)$. To wit,

(1) Discrete distribution of dislocation lines, in which case $p(y)=\Sigma_{n=1}^N \delta(y-y_n)$. This can be a periodic distribution, with $y_n=nh$ ($Nh=D$) or a random distribution with the $N-y_n$ values randomly distributed in $[-D/2,D/2]$.

(2) Continuous distributions, among which $p(y)=1/h$ is the continuous extension of the periodic discrete distribution.

The choice of a particular distribution is expected to influence significantly the expression of the field scattered by one/several grain boundary/ies in Eq. (2.3) only when the wavelength is comparable to the distance among dislocations within the grain boundary. However, when the interest is in the characterization of the effective medium (namely the attenuation and the velocity change), many grain boundaries are considered and an ensemble average is performed over all the parameters describing the grain boundaries. It will be seen that this average smoothes the differences between the different distributions $p(y)$: The result at first order is independent of the choice of $p(y)$ and at second order, the limit $kD<1$ is found to be roughly independent of $p(y)$.

Combining Eqs. (2.2) and (2.3) leads to a wave equation with a source ("potential") term

$$\rho\frac{\partial^2}{\partial t^2}v_i(\mathbf{x},t) - c_{ijkl}\frac{\partial^2}{\partial x_j\,\partial x_l}v_k(\mathbf{x},t) = V_{ik}v_k, \tag{2.5}$$

where

$$V_{ik}(\mathbf{x},\omega) = \frac{2}{L}\frac{(\mu b)^2}{m}\mathsf{M}_{ip}\mathsf{M}_{jk}\int dy\, p(y)d\sigma d\sigma'\frac{\partial}{\partial x_p}\delta[\mathbf{x}-\mathbf{X}(\sigma,y)] \times\sum_n p_n(\omega)\chi_n(\sigma)\chi_n(\sigma')\left.\frac{\partial}{\partial x_k}\right|_{\mathbf{x}=\mathbf{X}(\sigma',y)}. \tag{2.6}$$

B. Derivation of the modified wave numbers

The derivation of the potential in Eq. (2.6) allows one to treat the problem of the propagation of elastic waves through a polycrystal following a usual multiple scattering theory. Let us consider a configuration with an ensemble of grain boundaries described by a set of parameters (the position and the orientation of the boundaries for instance). This realization is described by a potential $V^T=\Sigma_i V^i$ in the wave equation as in Eq. (2.5), with V^i the potential of the ith grain boundary, as given in Eq. (2.6).

The problem can be formulated in terms of the modified Green tensor $\langle G\rangle$, that gives the impulse response of the medium averaged over all realizations of disorder, the average being taken over the set of parameters that describe a given configuration. The multiple scattering theory gives the modified Green tensor in the Dyson equation:[42–44]

$$\langle G\rangle = [(G^0)^{-1}-\Sigma]^{-1},$$

where Σ is the so-called mass operator related to the potential. The main difficulty in solving the Dyson equation is to find Σ but a closed form can be written if an approximation of Σ is performed for weak scattering. In that case, Σ can be expanded and, up to second order in a small parameter that measures the scattering strength, we have

$$\Sigma^{(1)} = \langle V^T \rangle,$$
$$\Sigma^{(2)} = \langle V^T G^0 V^T \rangle - \langle V^T \rangle G^0 \langle V^T \rangle. \tag{2.7}$$

In the case where V^T is a sum of individual potentials and assuming no correlations between the scatterers (that is no correlation between the parameters that define the disorder), the mass operator takes a simpler form as a function of the potential for a single scatterer. In Fourier space, this is written as

$$\Sigma_{ij}^{(1)}(\mathbf{k}) = n \int d\mathbf{x} d\mathbf{C}\, e^{-i\mathbf{kx}} V_{ij}(\mathbf{x}) e^{i\mathbf{kx}},$$
$$\Sigma_{ij}^{(2)}(\mathbf{k}) = n \int d\mathbf{x} d\mathbf{x}' d\mathbf{C}\, e^{-i\mathbf{kx}} V_{in}(\mathbf{x}) \times G_{nl}^0(\mathbf{x}-\mathbf{x}') V_{lj}(\mathbf{x}') e^{i\mathbf{kx}'}, \tag{2.8}$$

where n is the density of scatterers and where the integral over $d\mathbf{C}$ corresponds to the average over all the parameters of disorder.

In our calculation, (1) all elementary dislocation lines have the same Burgers vector b and the same mass per unit length m and (2) all grains have the same dimension $L \times D$. What differs from one grain boundary to the other is (3) the grain boundaries have different line spacing h, or equivalently different N values. This allows one to account for different misorientations between adjacent grains since a growing misorientation angle is expected to produce a decreasing line spacing and (4) the grain boundaries have random position and random orientations. To simplify the calculations, assumptions (3) is reduced to its simplest form where h can take any value in the interval $[\bar{h}-\Delta h, \bar{h}+\Delta h]$, with $\Delta h \ll \bar{h}$ [implying, for all f functions, $\langle f(h) \rangle \simeq f(\bar{h})$]. In summary, a realization of disorder corresponds to many grain boundaries of same size (dislocation walls), with density n, randomly distributed and orientated in an elastic medium (otherwise homogeneous and isotropic) with different (low) misorientation angles.

The whole task is now to derive the wave numbers $K_{L,T}$ of the modified Green function $\langle G \rangle$. The details of the calculations are reported in Appendix A and we find, for $\mathbf{k} = k\mathbf{e}_3$

$$\langle G \rangle^{-1}(\mathbf{k}) = G_0^{-1}(\mathbf{k}) - \Sigma(\mathbf{k}) = \rho c_T^2 \begin{pmatrix} (k^2 - k_T^2) & 0 & 0 \\ 0 & (k^2 - k_T^2) & 0 \\ 0 & 0 & \gamma^2 (k^2 - k_L^2) \end{pmatrix} - \rho c_T^2 k^2 \begin{pmatrix} F_{1T}(k,\omega) + F_{2T}(k,\omega) & 0 & 0 \\ 0 & F_{1T}(k,\omega) + F_{2T}(k,\omega) & 0 \\ 0 & 0 & F_{1L}(k,\omega) + F_{2L}(k,\omega) \end{pmatrix}. \tag{2.9}$$

With the notations

$$x \equiv \frac{\omega}{\omega_1}, \quad v \equiv kL/\pi, \tag{2.10}$$

$B_c \equiv 2m\omega_1$, and $\beta \equiv B/B_c$, the first-order terms are

$$F_{1T} \equiv \frac{2}{\pi^4} \frac{D}{\bar{h}} nL^3 \int_0^1 du (1-u^4) S(uv,x),$$
$$F_{1L} \equiv \frac{4}{\pi^4} \frac{D}{\bar{h}} nL^3 \int_0^1 du (1-u^2)^2 S(uv,x), \tag{2.11}$$
$$S(uv,x) \equiv \sum_j \frac{f_j(\pi uv/2)}{j^2(j^2 - x^2 - 2ix\beta)[(uv/j)^2 - 1]^2},$$

where $f_j \equiv \sin^2$ for j even and $f_j = \cos^2$ for j odd. This result at first order is independent of the distribution law $p(y)$ for the dislocation lines along the grain boundaries. This is because the first-order calculation corresponds to single scattering process averaged over all possible positions and orientations of the grain boundaries. The average causes the particular organization encapsulated in $p(y)$ to disappear. The calculation at second order, however, does depend on the choice on $p(y)$ since it involves a self-irradiation term: it is the contribution of the waves hitting twice the same scatterer. This contribution depends on the structure of the scatterer [here on $p(y)$], and the sum of waves hitting successively two dislocation lines of the same grain boundary will be different when, say, the line spacing is constant or random, since interferences are expected. The second-order terms are

$$F_{2T} \equiv \frac{i}{2\pi^7} \left(\frac{D}{\bar{h}} \right)^2 nL^3 x^3 \int_{-1}^1 du [\cos^2 \xi u^2 + \sin^2 \xi (1-2u^2)^2] \times \int_{-1}^1 da\, h_x(a,u) \int_0^{2\pi} d\xi\, g_x(\xi,u),$$
$$F_{2L} \equiv \frac{4i}{\pi^7} \left(\frac{D}{\bar{h}} \right)^2 nL^3 x^3 \int_{-1}^1 du\, u^2 (1-u^2) \times \int_{-1}^1 da\, h_x(a,u) \int_0^{2\pi} d\xi \sin^2 \xi\, g_x(\xi,u), \tag{2.12}$$

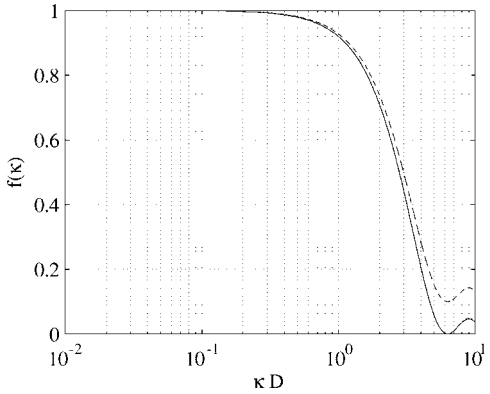

FIG. 3. Plots of the function $f(\kappa D)$ appearing at the second-order calculation in h_x in Eq. (2.12) for different distribution laws of the dislocation lines along the grain boundary. Full line; continuous distribution; dotted line (almost indistinguishable from the full line); discrete periodic distribution; dashed line; discrete random distribution. This plot considers for $D/\bar{h}=10$.

$$h_x(a,u) \equiv (1-3a^2+4a^4) f[(k_T a - ku)D] + \frac{4}{\gamma^5} a^2(1-a^2) f[(k_L a - ku)D],$$

$$g_x(\xi,u) \equiv R[S(\sqrt{1-u^2}\cos\xi v, x)]^2.$$

The function f appearing in h_x in Eq. (2.12) depends on $p(y)$ and we found

(1) $f(\kappa D)=\mathrm{sinc}^2(\kappa D/2)$ for a continuous distribution [with $\mathrm{sinc}(x)\equiv \sin x/x$].
(2) $f(\kappa D)=[\sin(\kappa D/2)/(D/\bar{h})\sin(\kappa\bar{h}/2)]^2$, characteristic of interference pattern produced by periodic arrays, for a discrete periodic distribution.
(3) $f(\kappa D)=[1-\mathrm{sinc}^2(\kappa D/2)]\bar{h}/D+\mathrm{sinc}^2(\kappa D/2)$ for a discrete random distribution.

Note that $f(\kappa D)$ tends to unity for $\kappa D \ll 1$ whatever the form of $p(y)$. The function f are quite the same for the continuous distribution and for the discrete periodic one, as it can be seen in Fig. 3.

Since the effective wave numbers $K_a, a=L,T$, are expected to be close to the undisturbed wave numbers k_a, we easily find, using $v(k_T)=x$ and $v(k_L)=x/\gamma$,

$$K_T \simeq k_T\left[1+\frac{1}{\pi^4}\frac{D}{\bar{h}} nL^3\left(f_{1T}(x)+\frac{i}{4\pi^3}\frac{D}{\bar{h}} f_{2T}(x)\right)\right],$$
$$K_L \simeq k_L\left[1+\frac{2}{\gamma^2\pi^4}\frac{D}{\bar{h}} nL^3\left(f_{1L}(x)+\frac{i}{\pi^3}\frac{D}{\bar{h}} f_{2L}(x)\right)\right], \tag{2.13}$$

with

$$f_{1T}(x) \equiv \int_0^1 du(1-u^4)S(ux,x),$$

$$f_{1L}(x) \equiv \int_0^1 du(1-u^2)^2 S(ux/\gamma,x),$$

$$f_{2T} \equiv x^3 \int_{-1}^{1} du[\cos^2\xi u^2 + \sin^2\xi(1-2u^2)^2] \times \int_{-1}^{1} da\, h_{xT}(a,u) \int_0^{2\pi} d\xi\, g_{xT}(\xi,u),$$

$$f_{2L} \equiv x^3 \int_{-1}^{1} du\, u^2(1-u^2) \int_{-1}^{1} da\, h_{xL}(a,u) \times \int_0^{2\pi} d\xi\, g_{xL}(\xi,u), \tag{2.14}$$

$$h_{xT}(a,u) \equiv (1-3a^2+4a^4) f[\pi x r(a-u)] + \frac{4}{\gamma^5} a^2(1-a^2) f[\pi x r(a/\gamma - u)],$$

$$h_{xL}(a,u) \equiv (1-3a^2+4a^4) f[\pi x r(a-u/\gamma)] + \frac{4}{\gamma^5} a^2(1-a^2) f[\pi x r(a-u)/\gamma],$$

$$g_{xT}(\xi,u) \equiv R[S(\sqrt{1-u^2}\cos\xi x, x)]^2,$$

$$g_{xL}(\xi,u) \equiv \sin^2\xi R[S(\sqrt{1-u^2}\cos\xi x/\gamma, x)]^2,$$

where $r\equiv D/L$. The previous expressions simplify considerably in the limit $x \ll 1$ of low frequencies, as will be seen in Sec. III B. Also, in that limit, it is easy to see that the case of isolated dislocation segments studied in Ref. 15 is recovered for $D/h=1, kD \ll 1$, in agreement with the fact that, for long wavelengths, the wave will see the grain boundary as a single, fat, dislocation segment.

III. VELOCITY CHANGES AND ATTENUATIONS

A. General expression of the velocity changes and attenuations

The attenuations $\alpha_a \equiv \mathrm{Im}[K_a]$ and modified velocity $v_a = \omega/R[K_a] (a=L,T)$ can be simply deduced from Eq. (2.13)

$$v_T \simeq c_T\left[1-\frac{1}{\pi^4}\frac{D}{\bar{h}} nL^3 R[f_{1T}(x)]\right],$$
$$v_L \simeq c_L\left[1-\frac{2}{\gamma^2\pi^4}\frac{D}{\bar{h}} nL^3 R[f_{1L}(x)]\right]. \tag{3.1}$$

and the attenuation

$$\alpha_T \simeq \frac{1}{\pi^3}\frac{D}{\bar{h}} nL^2 x\left[\mathrm{Im}[f_{1T}(x)] + \frac{1}{4\pi^3}\frac{D}{\bar{h}} f_{2T}(x)\right],$$
$$\alpha_L \simeq \frac{2}{\gamma^3\pi^3}\frac{D}{\bar{h}} nL^2 x\left[\mathrm{Im}[f_{1L}(x)] + \frac{1}{\pi^3}\frac{D}{\bar{h}} f_{2L}(x)\right]. \tag{3.2}$$

Typical behaviors of the attenuation and velocity change $\Delta v_a \equiv c_a - v_a$ are shown on Fig. 4 (technical details about the numerical calculations are given in Appendix B). We found two regimes, depending on the value of the drag B compared

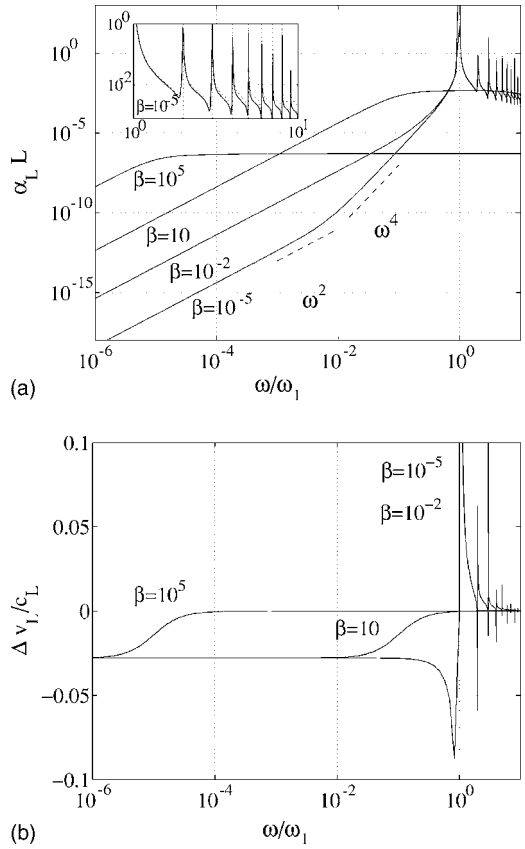

FIG. 4. Typical behaviors of (a) the attenuation $\alpha_L L$ and of (b) the velocity change $\Delta v_L/c_L$ as a function of the frequency, in the underdamped regime ($\beta=B/B_c=10^{-5},10^{-2}$) and in the overdamped regime ($B/B_c=10,10^{-5}$). Calculations have been performed using $nL^3=1$, $D/\bar{h}=10$ and $\gamma=2$ in Eqs. (3.1) and (3.2). (a) Calculations of the attenuation have been performed considering a continuous distribution of dislocation lines $p(y)$ along the grain boundaries. For $\beta=10^{-5}$ and 10^5, calculations have been performed for the discrete distributions $p(y)$ (periodic and random). The curves are superimposed but indiscernible. The inset shows a zoom for $\omega>\omega_1, \beta=10^{-5}$: the cases that are continuous (in plain line) and periodic (in dashed line) are still indiscernible. The case of discrete random distribution is represented in dotted line and here has the maximum difference 50% (otherwise lower than 0.15%). The ω^2 and ω^4 frequency laws are given for a guide to the eye.

with the critical value $B_c \equiv m\omega_1$ that fixes the limit of the over- and underdamped regimes for the dislocation motion. In the underdamped regime ($\beta \equiv B/B_c < 1$), the frequency law for the attenuation is a combination of a quadratic and quartic terms at low frequencies $\omega/\omega_1 < 1$. Above ω_1, resonances appear for incident wavelengths that are a submultiple of the grain size $L(\omega=n\omega_1)$. These resonances are smoothed because of the damping (encapsulated in B) and increasing $\beta \propto B$ causes them to disappear in the overdamped regime $\beta > 1$. A more detailed discussion on these regimes can be found in Ref. 15. The attenuation involves the second-order calculation. Calculations have been performed with the different distribution laws $p(y)$: continuous, periodic, and random. The difference between the three $p(y)$ laws decreases increasing β. This is because the second-order contribution is independent of β and increasing β makes the first-order contribution dominant [otherwise independent of $p(y)$]. For $\beta=10^{-5}$, the difference between the α values is lower than 0.15% for $\omega<\omega_1$. It reaches 50% for $\omega>\omega_1$, as shown in the inset of Fig. 4(a). For $\beta=10^5$, the differences between the α values is lower than 10^{-3}% in the whole frequency range $[10^{-6}-10]\omega_1$.

From these figures, the limit of validity of the present calculations can be commented upon. Our approach assumes that the multiple scattering medium behaves as an effective dissipative medium in which a coherent wave propagates, and a perturbative development is performed. This implies $\Delta v/c \ll 1$ and $\alpha/k \ll 1$, both conditions being a consequence of the perturbative method. It can be seen that, in the underdamped regime, frequencies $\omega > \omega_1$ give high attenuation and velocity change because of the resonances. In that regime, the weak scattering approximation will cease to be valid.

B. Velocity change and attenuation in the low frequency regime

In the low frequency regime ($\omega \ll \omega_1$ or $x \ll 1$), the expressions for velocity change simplify to

$$\frac{\Delta v_a}{c_a} \simeq \mathcal{C}_a \frac{D}{\bar{h}} nL^3 \frac{1}{1+x^2\beta^2}, \tag{3.3}$$

with $C_T=4/(5\pi^4), C_L=16/(15\gamma^2\pi^4)$, and for attenuation to

$$\alpha_a \simeq \mathcal{D}_a \frac{D}{\bar{h}} nL^2 x^2 \left[\frac{\beta}{1+x^2\beta^2} + \frac{4}{15\pi^2} \frac{3\gamma^5+2}{\gamma^5} \frac{D}{\bar{h}} \frac{x^2(1-x^2\beta^2)}{(1+x^2\beta^2)^2} \right], \tag{3.4}$$

with $\mathcal{D}_T=4/(5\pi^3)$, $\mathcal{D}_L=16/(15\gamma^3\pi^3)$, and $\beta=B/B_c$. These results agree with those obtained for isolated dislocation segments in Ref. 15 with the replacements $b \to \bar{N}b$ and $m \to \bar{N}m$ with $\bar{N} \equiv D/\bar{h}$ the number of dislocation segments held in a grain boundary [or equivalently $D/\bar{h}=1$]. This reasonably means that a grain boundary behaves as a single (fat) dislocation segment with total Burgers vector $\bar{N}b$ and total mass $\bar{N}m$ in the low frequency regime. The behaviors in the under- or overdamped regimes are illustrated in Fig. 4 and a discussion can be found in Ref. 15. In the underdamped regime, the terms $x\beta \ll 1$ vanish and the attenuation has simply a contribution in x^2 due to the drag $B \propto \beta$ and a contribution in x^4 due to multiple scattering process. This behavior is compared with experimental results in Sec. IV.

IV. COMPARISON WITH ZHANG *et al.* EXPERIMENTS

In a recent publication, Zhang *et al.*[12] have reported the experimental measurement of the attenuation of longitudinal waves with frequencies in the 10 MHz range (meaning wavelengths of the order of millimeter) in polycrystalline copper. The care taken by these authors to prepare the samples allowed them to characterize very accurately the frequency dependence, and the data clearly exhibit, in addition to the usual quartic law, a quadratic term. The data fits reported in that paper are discussed in this section.

Following Zhang's notation, we write $\alpha=\alpha_L(c=c_L)$ and

TABLE I. Coefficients of the fits for the attenuation in $\alpha=\alpha_2 f^2+\alpha_4 f^4$, from Zhang *et al.* (Ref. 12) for different grain sizes d in different prepared samples (PM and CW). Two sets of values for h and B/b^2 are reported, The first ($V1$) correspond to the values deduced from Eq. (4.2) in the polynomial approximation and the second [($V2$) in parentheses] are the values that give the best fits between our complete expression α^{th} [Eq. (3.2)] and the polynomial expansion given by Zhang.

Sample reference (in Ref. 12)	PM3		PM5		CW2		CW4	
d (μm)	9.77		26.9		10.3		33.9	
α_2 (10^{-15} m^{-1} Hz^{-2})	12		32		71		240	
α_4 (10^{-30} m^{-1} Hz^{-4})	9		180		7		280	
$\bar{h}$ (μm)	1.25	(0.79)	3.52	(2.41)	1.62	(1.98)	5.03	(11.24)
B/b^2 (10^{13} Pa s m^{-2})	0.039	(0.025)	0.0140	(0.0110)	0.254	(0.309)	0.075	(0.168)

$$\alpha = P(f) = \alpha_2 f^2 + \alpha_4 f^4. \tag{4.1}$$

Now, our expression (3.4) in the limit $x \ll 1$ and in the underdamped regime gives the same polynomial expansion as Eq. (4.1) with the identifications

$$\alpha_2 = \frac{64}{15\pi^4}\frac{BnL^5}{\rho b^2 c^3}\frac{D}{\bar{h}},$$
$$\alpha_4 = \frac{1024}{225\pi^5}\frac{3\gamma^5+2}{\gamma^4}\frac{nL^6}{c^4}\left(\frac{D}{\bar{h}}\right)^2. \tag{4.2}$$

Note the proportionality of α_2 with D. The latter is a linear dimension associated with grain boundary size, which it is not unreasonable to suppose proportional to grain size. In this case this formula provides a rationale for the linear scaling between α_2 and grain size found by Zhang *et al.*[12]

We have to introduce simplifying assumptions concerning grain shape that should not affect measurements performed at length scales much larger than grain size:

(1) Following Zhang *et al.*, we shall call d the grain size, and we shall assume it is of the same order of magnitude as all dimensions of the grain boundaries, or, in the language of the present model, the dislocation walls: $d \approx L \approx D \approx w$.
(2) With the previous assumption, we assume $nd^3 \sim 1$, which means that the grains are "cubes" uniformly distributed throughout space.

With these assumptions it is possible to find simplified expressions with only two undetermined parameters: $\bar{h}$, the mean distance between two dislocations within a grain boundary, and B/b^2, a ratio that depends on the characteristics of the dislocation in the grain boundary:

$$\alpha_2 = \frac{64}{15\pi^4}\frac{d^3}{\rho c^3}\frac{B}{b^2}\frac{1}{\bar{h}}, \quad \alpha_4 = \frac{1024}{225\pi^5}\frac{3\gamma^5+2}{\gamma^4}\frac{d^5}{c^4}\frac{1}{\bar{h}^2}. \tag{4.3}$$

Equation (4.3) does not contradict the linear scaling with D predicted by our model. It is a consequence of the assumption $L \sim D \sim w$, which is used for the numerical estimations of Table I.

For two sets of samples denoted PM (prepared by the power metallurgy method) and CW (cast-and-wrought), Zhang *et al.* give the coefficients of the polynomial fits of the experimental data [α_2 and α_4 defined in $P(f)$, Eq. (4.1)]. These results are reported in Table I, together with the values of $\bar{h}$ and of (B/b^2) they imply in our model when the polynomial simplification is considered [Eq. (4.1)]. To do that, it is sufficient to use the above-presented expression of α_4 in Eq. (4.3) to determine $\bar{h}$ without any adjustable parameters

$$\bar{h} = \frac{1024}{225\pi^5}\frac{3\gamma^5+2}{\gamma^4}\frac{d^5}{c^4}\frac{1}{\alpha_4}. \tag{4.4}$$

This value of $\bar{h}$ can then be used in the expression of α_2 to extract the ratio B/b^2,

$$\left(\frac{B}{b^2}\right) = \frac{15\pi^4}{64}\frac{\rho c^3}{d^3}\alpha_2 \bar{h}^g. \tag{4.5}$$

Results are presented in Table I (values $V1$), for $\rho=9\times10^{-3}$ kg m^{-3}, $c=4900$ m s^{-1}, and $\gamma=2$.

The results for $\bar{h}$ seem eminently reasonable: The few micrometers found for the distance between dislocation corresponds to the value, first observed by Lacombe[45] and reported by Read and Shockley in 1950.[19] It corresponds to a low angle grain boundary with a disorientation angle of about 10^{-3} rad for b around 1 nm.

The results implied for B/b^2 however, differ from the values of B commonly accepted for an isolated dislocation. Indeed, in this case b is typically below the nanometer and B is around 10^{-5} Pa s at room temperature,[46–48] giving a value for the ratio B/b^2 around 10^{13} Pa s m^{-2} if the dislocation segments within a grain boundary behave as isolated dislocation segments. This is at least one order of magnitude above the results reported in Table I, reasonably suggesting that the presence of neighboring dislocation segments strongly affects their damping dynamics. In other words, keeping the usual value of b, the drag B of the dislocation segment in the grain boundary is found around 10^{-6} Pa s, a value significantly smaller than the value for an isolated dislocation. Finally, note that we can check the assumption made that the dislocations move in an underdamped regime since the ratio B/B_c is found to typically lie between 0.02 and 0.2.

Comment on the polynomial approximation. The validity of the polynomial approximation is measured by the difference with the exact theoretical expression α^{th} given in Eq. (3.2), whose approximated form is the polynomial approxi-

mation only for $x \ll 1$. Since the experimental configurations for PM3, PM4, CW4, and CW5 cover x between 0.08 and 0.5, the approximation may be questioned. We denote $\alpha^{\exp}$ the polynomial approximation [indeed, remember that the polynomial approximation with $\bar{h}$ and (B/b^2) in Eqs. (4.4) and (4.5) gives exactly the experimental results, by construction] and $E=|\alpha^{\text{th}}-\alpha^{\exp}|/|\alpha^{\exp}|$ the difference with the exact expression.

The difference E on the attenuation is as follows (a mean value is taken in the frequency range [10–18] MHz): For PM3 ($x<0.14, B/B_c=0.03$), we get $E=7\%$. For PM5 ($x<0.4, B/B_c=0.03$), $E=25\%$. For CW2 ($x<0.15, B/B_c=0.19$), $E=1.3\%$ and for CW4 ($x<0.5, B/B_c=0.18$), $E=16\%$. As expected, E increases as x increases. Figure 6 illustrates this behavior: We have represented the experimental attenuation (identical to the polynomial approximation) and α^{th} calculated with the values of $\bar{h}$ and B/b^2 in Eqs. (4.4) and (4.5) ($V1$ values). The maximum difference is observed for the PM5 sample.

We have performed a second calculation in which the $V1$ values $(\bar{h}, B/b^2)$ are taken as initial guess values. Then, these values have been adjusted to obtain the best agreement with the polynomial fits. To do that, we have searched a minimum of $E=|\alpha^{\text{th}}-\alpha^{\exp}|/|\alpha^{\exp}|$, where α^{th} is numerically calculated with two adjustable parameters B/b^2 and $\bar{h}$: The minimum of $E(B/b^2, \bar{h})$ is found in a two-dimensional space where B/b^2 and $\bar{h}$ have been centered on the initial guess value with 100% variation. Figure 5 illustrates the procedure.

The resulting values ($V2$) are also presented in Table I and in Fig. 6. The resulting error E is decreased, around 1% for all samples.

Note that the difference between values ($V1$) and ($V2$) is significant but, as expected for relatively small x values, it does not change the order of magnitude of $\bar{h}$ and B/b^2.

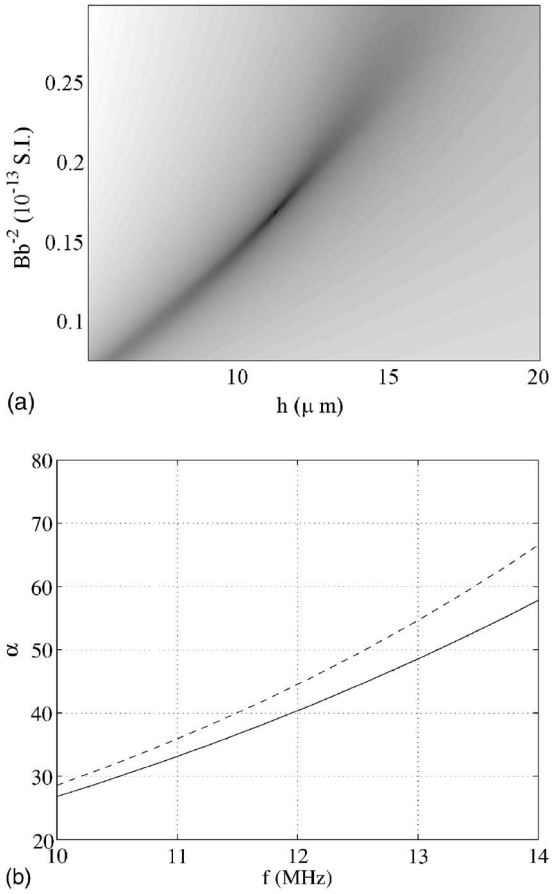

FIG. 5. (a) Example of the function error $E=|\alpha^{\text{th}}-\alpha^{\exp}|/|\alpha^{\exp}|$ [log(E) in gray scale] as a function of the two adjustable parameters B/b^2 and $\bar{h}$ (here for the case CW4 in Table I). White is the higher value (here 200%) and black the lowest value (0.08%). (b) The attenuation: in full line, the experimental fit given by Zhang *et al.* for CW4, in dotted line the attenuation calculated from Eq. (3.2) with the initial guess values $V1((B/b^2)=7.49\times10^{11}$ S.I. and $\bar{h}=5.0265$ μm and in dotted line, the best fit of the attenuation calculated from Eq. (3.2), obtained with the values $V2: B/b^2=16.81\times10^{11}$ S.I. and $\bar{h}=11.24$ μm.

V. COMMENT ON THE EFFECT OF GRAIN ANISOTROPY

The attenuation measured in polycrystals has been widely studied as originating from the variation in the elastic constants relevant for the propagation of waves from grain to grain due to the change in the grain orientation.[1–11] This effect can be encapsulated in a potential in the wave equation

$$\rho\frac{\partial^2}{\partial t^2}v_i(\mathbf{x},t)-\langle c_{ijkl}\rangle\frac{\partial^2}{\partial x_j\,\partial x_l}v_k(\mathbf{x},t)=V_{ik}^T(\mathbf{x})v_k(\mathbf{x},t),$$
$$V_{ik}^T(\mathbf{x})\equiv-\frac{\partial}{\partial x_j}\left(\delta c_{ijkl}(\mathbf{x})\frac{\partial}{\partial x_l}\,.\,\right), \tag{5.1}$$

where $\langle c_{ijkl}\rangle$ are the mean elastic constants, averaged over all possible orientations of the crystal axis, and $\delta c_{ijkl}(\mathbf{x})$ are the variations in the elastic constants from grain to grain, with respect to their mean value. In that case, the attenuation is found to be of the form

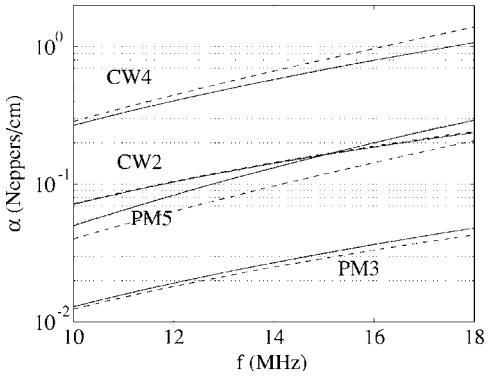

FIG. 6. Comparison with experiments reported in Zhang *et al.* for the four samples whose fits are given (see Table I): solid lines correspond to the experimental fitted curves. The correction of the simple power law in $\alpha_2 f^2+\alpha_4 f^4$ using the whole expression in Eq. (3.2) is given using $(B/b^2, \bar{h})$ coming from: in dashed line, the $V1$ values deduced from the polynomial approximation and in dotted line (almost superposed to the experimental curves) the $V2$ values minimizing the difference with the experimental configuration.

$$\alpha d \sim \mathcal{C}\left(\frac{\eta}{c_{11}}\right)^2\left(\frac{\omega d}{c_L}\right)^4, \tag{5.2}$$

where c_{11} is the first term of the stiffness matrix, equal to $\lambda+2\mu$ for isotropic media and $\eta=c_{11}-c_{12}-2c_{44}$ is a measure of the anisotropy of the single crystal. $\mathcal{C}$ is a numerical constant, of the order than $10^{-2}-10^{-3}$ (a simplified presentation of the calculation is given in Appendix C, for a more complete derivation of the Dyson equation, see Ref. 10). The contribution of the anisotropy of the crystal grain corresponds to a second-order contribution in the perturbative expansion, the first order vanishing because it is proportional to $\langle \delta c_{ijkl} \rangle$ that is zero, by definition.

It is shown in Appendix C that the attenuations due to the dislocations in the grain boundaries and due to the grain anisotropy simply superpose when both effects are considered. The attenuation could be thus written, with both effects,

$$\alpha d = \mathcal{A}\frac{B}{B_c}\frac{d}{\bar{h}}\left(\frac{\omega d}{c_L}\right)^2 + \left[\mathcal{B}\left(\frac{d}{\bar{h}}\right)^2 + \mathcal{C}\left(\frac{\eta}{c_{11}}\right)^2\right]\left(\frac{\omega d}{c_L}\right)^4, \tag{5.3}$$

where we have used the simplified expression in Eqs. (4.1)–(4.3): $\mathcal{A}=16/(15\gamma\pi^5)\simeq 2\times 10^{-3}$ and $\mathcal{B}=64(3\gamma^5+2)/(225\pi^9\gamma^4)\simeq 5\times 10^{-5}$. A comparison between the two quartic terms will depend on the characteristics of the material at hand. For copper, studied in Refs. 1 and 49, η is of the same order than the stiffness coefficients c_{ij}. With $d/\bar{h}\sim 10$ dislocations per grain boundary (as we have found in Table I), the two contributions are of the same order of magnitude. This means that including both effects in our study would not change significantly the results on the values of B and $\bar{h}$. Of course, this balance can change depending on the polycrystal.

VI. CONCLUDING REMARKS

Recent measurements of ultrasound attenuation can be understood in terms of a model that blames the attenuation on scattering by grain boundaries that are made of dislocation arrays. For low frequencies, that is, wavelengths long compared to grain size, the grain boundaries mainly behave as an ensemble of isolated dislocations, with an effective mass and an effective Burgers vector equal to the total mass and the total Burgers vector "held" by the grain boundary. A frequency law that is a linear combination of quadratic and quartic terms naturally appears. The quadratic term is due to the drag experienced by the dislocations as they respond to the externally generated acoustic wave. The quartic term is due to the damping experienced by the coherent wave as energy is taken from it by the randomly placed grain boundaries; it is an effect of disorder.

The quadratic scaling of the attenuation due to (individual) dislocation damping has been known since the 1950s[50–54] and the extra quartic contribution that appears when many, randomly located, dislocations are present, has been identified more recently.[15] In the low frequency regime, the quadratic contribution of the dislocations (say of length l) to the attenuation typically behaves as $\alpha\sim 10^{-3}\Lambda l\beta(\omega/\omega_1)^2$ with $\omega_1=\pi c/l$ the first resonance frequency and $\Lambda=nl$ the surface density of dislocations. This law has successfully explained the attenuation due to dislocations experimentally measured in the range of $10^{-2}-1$ m^{-1} (typical temporal attenuation, αc, being in the range $10^{-4}-10^{-2}$ μs^{-1} for ring-down curves).[55–61] The attenuations measured in the experiments of Zhang *et al.* are two orders of magnitude larger than in experiments that refer to dislocation damping, meaning that the contribution to the attenuation of the (individual) dislocations in the bulk of the grains can be neglected.

However, grain boundaries pictured as arrays of dislocations, a good approximation in the low-angle case, are good candidates to explain the quadratic term of the measured attenuation, with the dislocation drag significantly diminished by the presence of neighboring dislocations nearby. The quartic term can quite reasonably be understood as arising from the presence of many, randomly placed and oriented, grain boundaries, a quartic contribution that has to be compared with the usual contribution of the change in grain anisotropy.

Zhang *et al.*[12] found a difference in attenuation for samples prepared via powder metallurgy and equal channel angular extrusion, presumably linked to the difference in grain size distribution. In our work, while we can fit the data with appropriate values for the dynamic attenuation of dislocation motion B, we have taken an approximation in which grain boundaries, while randomly distributed, have identical sizes. Our formalism allows for a more general treatment with a more realistic distribution, and remains a possible direction for future work.

Finally, the dislocation walls that form grain boundaries appear to be good candidate as source of damping in polycrystals. Further measurements of the attenuation in a larger range of frequencies would be helpful (1) to confirm the results of Zhang *et al.* concerning the quadratic contribution in the low frequency regime, (2) to discriminate between the contribution due to the dislocation walls and due to the anisotropy in the transition (near ω_1) regime, and (3) to investigate the high frequency regime where resonances should be observed. Also, the low value of the drag coefficient that we obtain using the data of Zhang *et al.* needs to be further investigated if this result is confirmed.

ACKNOWLEDGMENTS

This work has been supported by ECOS Contract No. C04E01 and by FONDAP Grant No. 11980002. F.B. thanks Fondecyt Project No. 1060820. We are pleased to thank Erik Bitzek for fruitful discussions.

APPENDIX A: DERIVATION OF THE MASS OPERATOR

The task is here to derive the so-called mass operator Σ that links the modified Green tensor $\langle G \rangle$ of the effective medium (corresponding to an average of all realizations of the medium filled with random distributions of scatterers) and the Green tensor G^0 of the elastic medium free of scatterers. In the limit of weak scattering, the mass operator can be developed as in Eq. (2.8). In our case, the calculation is

performed up to second order. The first order gives the velocity change and a term of the attenuation due to internal viscosity (via the drag term B in the equation of motion for the dislocation) and the second order gives a term in the attenuation due to the energy that is taken away from the direction of propagation. This latter term exists even in the absence of any viscous effect.

To do the calculations, we restrict ourselves to the following assumptions:

(1) All the elementary dislocation lines along the grain boundary are identical, meaning they have the same Burger vector b and the same mass per unit length m.
(2) All grains have the same dimension $L \times D$.

The randomness has two sources:

(1) The grain boundaries hold different number N of dislocation lines, or equivalently different spacing h. This allows one to account for different misorientations between adjacent grains since a growing misorientation angle is expected to produce an increasing N value. We choose the simplest case where h can take any values in the interval $[\bar{h}-\Delta h, \bar{h}+\Delta h]$ with $\Delta h \ll \bar{h}$, thus we use $\langle f(h)\rangle \simeq f(\bar{h})$.
(2) The grain boundaries can have any orientation, the orientation of a grain being given by the orientation of the two vector $(\boldsymbol{\tau}, \mathbf{t})$. The two vector is described by the Euler angles (θ, φ, ξ). We denote R the rotation matrix $\mathsf{R}=\mathsf{R}(\mathbf{e}_3, \theta)\mathsf{R}(\mathbf{e}_2, \varphi)\mathsf{R}(\mathbf{e}_1, \xi)$,

$$\mathsf{R} = \begin{pmatrix} \cos\varphi\cos\theta & -\sin\theta\cos\xi - \sin\varphi\cos\theta\sin\xi & \sin\theta\sin\xi - \sin\varphi\cos\theta\cos\xi \\ \cos\varphi\sin\theta & \cos\theta\cos\xi - \sin\varphi\sin\theta\sin\xi & -\cos\theta\sin\xi - \sin\varphi\sin\theta\cos\xi \\ \sin\varphi & \cos\varphi\sin\xi & \cos\varphi\cos\xi \end{pmatrix} \tag{A1}$$

Also, when a discrete random distribution of dislocation lines is considered: $p(y)=\Sigma\delta(y-y_n)$, with y_n randomly distributed in $[-D/2, D/2]$, an additional average has to be performed to account for all possible positions of y_n. This is done through $\int dy_1 dy_2 \ldots dy_N/D^N$., indicating that each y_n has the D length as accessible space. Finally, the average over the orientations of the grain boundaries is encapsulated in the notation $\int d\mathbf{C}$.

1. First-order calculation

The first-order calculation is straightforward. We have, denoting $\chi_n(\sigma) \equiv \sin[(n\pi/L)(\sigma+L/2)]$ and $p_n(\omega) \equiv 1/(\omega^2 - \omega_n^2 + i\omega B/m)$,

$$\begin{aligned}\Sigma_{ij}^{(1)}(\mathbf{k}) &= n\int d\mathbf{x}d\mathbf{C}e^{-i\mathbf{kx}}V_{ik}(\mathbf{x})e^{i\mathbf{kx}} \\ &= \frac{2n}{L}\frac{(\mu b)^2}{m}\int d\mathbf{x}d\mathbf{C}dyp(y)d\sigma d\sigma' e^{-i\mathbf{kx}}\mathsf{M}_{ip}\mathsf{M}_{jq} \\ &\quad\times\frac{\partial}{\partial x_p}\delta[\mathbf{x}-\mathbf{X}(\sigma,y)]\sum_n p_n(\omega)\chi_n(\sigma)\chi_n(\sigma')\frac{\partial e^{i\mathbf{kx}}}{\partial x_{q|\mathbf{x}}} \\ &= -\frac{2n}{L}\frac{(\mu b)^2}{m}\int dyp(y)\int d\mathbf{C}\mathsf{M}_{ip}\mathsf{M}_{jq}k_pk_q \\ &\quad\times\sum_n p_n(\omega)\left|\int d\sigma\chi_n(\sigma)e^{i\mathbf{k}\cdot\boldsymbol{\tau}\sigma}\right|^2 \\ &= -\frac{4L^2}{\pi^2}\frac{2n}{L}\frac{D}{\bar{h}}\frac{(\mu b)^2}{m}\int d\mathbf{C}\mathsf{M}_{ip}\mathsf{M}_{jq}k_pk_q\sum_n a_n(\omega,\mathbf{k}\cdot\boldsymbol{\tau})\end{aligned}$$

where we have used $\int dyp(y)=N=D/h$ for any distribution of dislocation lines and where

$$\begin{aligned}a_n(\omega,k) &\equiv \frac{\sin^2(kL/2)}{[(kL/n\pi)^2-1]^2}\frac{p_n(\omega)}{n^n} \quad \text{for } n \text{ even} \\ &\equiv \frac{\cos^2(kL/2)}{[(kL/n\pi)^2-1]^2}\frac{p_n(\omega)}{n^n} \quad \text{for } n \text{ odd.}\end{aligned} \tag{A2}$$

The integration over $\mathbf{C}$ has to be performed over the Euler angles (θ, φ, ξ) since we have to account for all orientations of the two vectors $(\boldsymbol{\tau}, \mathbf{b})$. We denote R the rotation matrix $\mathsf{R} \equiv \mathsf{R}(\mathbf{e}_3, \theta)\mathsf{R}(\mathbf{e}_2, \varphi)\mathsf{R}(\mathbf{e}_1, \xi)$,

$$\mathsf{R} = \begin{pmatrix} \cos\varphi\cos\theta & -\sin\theta\cos\xi - \sin\varphi\cos\theta\sin\xi & \sin\theta\sin\xi - \sin\varphi\cos\theta\cos\xi \\ \cos\varphi\sin\theta & \cos\theta\cos\xi - \sin\varphi\sin\theta\sin\xi & -\cos\theta\sin\xi - \sin\varphi\sin\theta\cos\xi \\ \sin\varphi & \cos\varphi\sin\xi & \cos\varphi\cos\xi \end{pmatrix} \tag{A3}$$

Without loss of generality, we choose $\boldsymbol{\tau}=\mathsf{R}\mathbf{e}_1, \mathbf{t}=\mathsf{R}\mathbf{e}_2, \mathbf{n}=\mathsf{R}\mathbf{e}_3$ and we choose arbitrarily $\mathbf{k}=k\mathbf{e}_3$ (the general form of the modified Green function can be obtained through rotations afterwards if desired). We obtain

$$\Sigma^{(1)}(\mathbf{k}) = -k^2 \frac{4L^2}{\pi^2} \frac{2nD}{L\bar{h}} \frac{(\mu b)^2}{m} \int d\mathbf{C}\mathbf{V}^t\mathbf{V} \sum_n a_n(\omega, k\mathsf{R}_{31}),$$

with $V_i \equiv \mathsf{R}_{i3}\mathsf{R}_{32}+\mathsf{R}_{i2}\mathsf{R}_{33}$. Since $\mathsf{R}_{31}=\sin\varphi$ is independent of θ and ξ in f_n, it is easy to integrate over θ and ξ. This allows one to show that $\Sigma^{(1)}$ is diagonal with $\Sigma^{(1)}_{11}=\Sigma^{(1)}_{22}$. We denote $\Sigma^{(1)}_T \equiv \Sigma^{(1)}_{11}$ and $\Sigma^{(1)}_L \equiv \Sigma^{(1)}_{33}$,

$$\Sigma^{(1)}_T(k) = -\rho c_T^2 k^2 \frac{D}{\bar{h}} \frac{nLc_T^2}{2} \int_0^1 du(1-u^4) \sum_n a_n(\omega, ku),$$

$$\Sigma^{(1)}_L(k) = -\rho c_T^2 k^2 \frac{D}{\bar{h}} nLc_T^2 \int_0^1 du(1-u^2)^2 \sum_n a_n(\omega, ku),$$

where we have used $\mu=\rho c_T^2$.

2. Second-order calculation

Calculations at second order are quite long but similar to the first-order ones. We report here the main steps of these calculations,

$$\begin{aligned}
\Sigma^{(2)}_{ij}(\mathbf{k}) &= n \int d\mathbf{x} d\mathbf{x}' d\mathbf{C} e^{-i\mathbf{k}\mathbf{x}} V_{in}(\mathbf{x}) G^0_{nl}(\mathbf{x}-\mathbf{x}') V_{lj}(\mathbf{x}') e^{i\mathbf{k}\mathbf{x}'} \\
&= \frac{4n}{L^2} \frac{(\mu b)^4}{m^2} \int d\mathbf{x} d\mathbf{x}' d\mathbf{C} \mathsf{M}_{ip} \mathsf{M}_{nq} \mathsf{M}_{lr} \mathsf{M}_{jt} \\
&\quad \times \int dy p(y) d\sigma d\sigma' dy' p(y') ds ds' e^{i\mathbf{k}\mathbf{x}} \frac{\partial}{\partial x_p} \\
&\quad \times \delta[\mathbf{x}-\mathbf{X}(\sigma,y)] \sum_n pn \chi_n(\sigma) \chi_n(\sigma') \\
&\quad \times \frac{\partial}{\partial x_{k|\mathbf{x}=\mathbf{X}(\sigma',y)}} G^0_{nl}(\mathbf{x}-\mathbf{x}') \frac{\partial}{\partial x'_r} \delta[\mathbf{x}'-\mathbf{X}(s,y')] \\
&\quad \times \sum_m p_m \chi_m(s) \chi_m(s') \frac{\partial e^{i\mathbf{k}\mathbf{x}'}}{\partial x'_{t|\mathbf{x}'=\mathbf{X}(s',y')}}.
\end{aligned}$$

We use $G^0(\mathbf{x}) = 1/(2\pi)^3 \int d\mathbf{q} G^0(\mathbf{q}) e^{i\mathbf{q}\mathbf{x}}$ and $\mathbf{X}(\sigma,y)=\sigma\boldsymbol{\tau}+y\mathbf{n}$ to get

$$\begin{aligned}
\Sigma^{(2)}_{ij}(\mathbf{k}) &= \frac{4n}{(2\pi)^3 L^2} \frac{(\mu b)^4}{m^2} \left(\frac{4L^2}{\pi^2}\right)^2 \\
&\quad \times \int d\mathbf{q} d\mathbf{C} \mathsf{M}_{ip} \mathsf{M}_{nq} \mathsf{M}_{lr} \mathsf{M}_{jt} q_q k_t k_q q_r G^0_{nl}(\mathbf{q}) \\
&\quad \times \left| \int dy p(y) e^{i(\mathbf{k}-\mathbf{q})\mathbf{n}y} \right|^2 \\
&\quad \times \sum_n a_n(\omega, \mathbf{k}\boldsymbol{\tau}) \sum_m a_m(\omega, \mathbf{k}\boldsymbol{\tau}),
\end{aligned}$$

which can be written without indices in a more tractable form

$$\begin{aligned}
\Sigma^{(2)}(\mathbf{k}) &= \frac{4n}{(2\pi)^3 L^2} \frac{(\mu b)^4}{m^2} \left(\frac{4L^2}{\pi^2}\right)^2 \left(\frac{D}{\bar{h}}\right)^2 k^2 \\
&\quad \times \int d\mathbf{q} d\mathbf{C} \mathcal{A} \mathbf{V}^t\mathbf{V} f[(\mathbf{k}-\mathbf{q})\cdot\mathbf{n}D] g(\mathbf{k}\cdot\boldsymbol{\tau}),
\end{aligned}$$

where $\mathcal{A} \equiv {}^t\mathbf{q}\mathsf{M}G^0(\mathbf{q})\mathsf{M}\mathbf{q}$ is a scalar term, $\mathbf{V} \equiv \mathsf{M}\hat{\mathbf{k}}$ is a vector and with $g(x) \equiv |\Sigma_n a_n(x)|^2$.

The function f depends on the distribution law considered for the dislocation lines. With

$$f(\kappa D) \equiv \left(\frac{\bar{h}}{D}\right)^2 \left\langle \left| \int_{-D/2}^{D/2} dy p(y) e^{i\kappa x} \right|^2 \right\rangle, \tag{A4}$$

where $\langle\cdot\rangle$ denotes the average over h and for the discrete random distribution, the average over the positions of the dislocation on a single grain boundary.

Let us give the expression of the function f for the continuous or discrete distributions $p(y)$:

(1) For a continuous distribution $p(y)=1/h$, it is easily found, with $\mathrm{sinc}\, X \equiv \sin X/X$,

$$f(\kappa D) = \mathrm{sinc}^2(\kappa D/2). \tag{A5}$$

(2) For a discrete periodic distribution $p(y)=\sum_{n=1}^N \delta(y-nh)$, with $D=Nh$, the integral is easily obtained

$$f(\kappa D) = \left[\frac{\sin(\kappa D/2)}{(D/\bar{h})\sin(\kappa\bar{h}/2)} \right]^2. \tag{A6}$$

(3) For a discrete random distribution $p(y)=\sum_{n=1}^N \delta(y-y_n)$ with y_n randomly distributed in $[-D/2, D/2]$, an additional average has to be performed. Denoting $\bar{N}=D/\bar{h}$, we get

$$\begin{aligned}
f(\kappa D) &= \frac{1}{\bar{N}^2} \int dh \int dy dy' \int \frac{dy_1 \cdots dy_N}{D^N} \\
&\quad \times \sum_{n=1}^N \delta(y-y_n) \sum_{m=1}^N \delta(y'-y_m) e^{i\kappa(y-y')} \\
&= \frac{1}{\bar{N}^2} \int dh \int \frac{dy_1 \cdots dy_N}{D^N} \sum_{n,m=1}^N e^{i\kappa(y_n-y_m)} \\
&= \frac{1}{\bar{N}^2} \int dh \left[N \int \frac{dy_1}{D} + N(N-1) \right. \\
&\quad \left. \times \int \frac{dy_1 dy_2}{D^2} e^{i\kappa(y_1-y_2)} \right] \\
&= \frac{\bar{h}}{D}[1-\mathrm{sinc}^2(\kappa D/2)] + \mathrm{sinc}^2(\kappa D/2).
\end{aligned} \tag{A7}$$

The typical behavior of these functions is illustrated in Fig. 3.

We choose now $\boldsymbol{\tau}=\mathsf{R}\mathbf{e}_3, \mathbf{t}=\mathsf{R}\mathbf{e}_2, \mathbf{n}=\mathsf{R}\mathbf{e}_1$, and still $\mathbf{k}=k\mathbf{e}_3$. The above-mentioned integrals can be rewritten (with a change of variable $\mathbf{q} \to {}^t\mathsf{R}\mathbf{q}$)

$$\Sigma^{(2)}(\mathbf{k}) = \frac{4n}{(2\pi)^3 L^2}\frac{(\mu b)^4}{m^2}\left(\frac{4L^2}{\pi^2}\right)^2 k^2 \times \int d\mathbf{q} d\mathbf{C} \mathcal{A}\mathbf{V}^t\mathbf{V} f[k\mathsf{R}_{31} - q\hat{\mathbf{q}}_1] g(k\mathsf{R}_{33}).$$

with $\mathcal{A} \equiv {}^t\mathbf{q}\mathsf{M}_{12}G^0(\mathbf{q})\mathsf{M}_{12}\mathbf{q}(\mathsf{M}_{12} \equiv \mathbf{e}_1{}^t\mathbf{e}_2 + \mathbf{e}_2{}^t\mathbf{e}_1)$ and $\mathbf{V} \equiv \mathsf{M}\mathbf{e}_3$.

In the absence of the functions f and g, the integrals over $\mathbf{C}$ and $\mathbf{q}$ would be separable since $\mathcal{A}$ depends only on $\mathbf{q}$ and $\mathbf{V}$ only on the Euler angles described by $\mathbf{C}$. As in the calculation of the mass operator at first order, the choice of $\mathbf{k}$ along $\mathbf{e_3}$ and $\mathbf{n}$ is motivated by the fact that $\mathsf{R}_{31} = \sin\varphi$ (appearing in the coupling function f) allows the direct integration over the two other Euler angles (θ, ξ). Here, because we have to deal with $\mathbf{k}\cdot\boldsymbol{\tau}$ and $\mathbf{k}\cdot\mathbf{n}$, we have to let in the coupling functions at least one other Euler angle: it appears in g through $\mathsf{R}_{33} = \cos\varphi\cos\xi$. It is thus possible to integrate freely the operator $\mathbf{V^t V}$ only over θ.

In a similar way, the integration of $\mathcal{A}$ over $\mathbf{q}$ can be performed singly $(\hat{\mathbf{q}}_2, \hat{\mathbf{q}}_3)$ since the coupling function f involves only $\hat{\mathbf{q}}_1$ and we choose the angles (α, β), such $\hat{\mathbf{q}}_1 = \sin\alpha$, $\hat{\mathbf{q}}_2 = \cos\alpha\cos\beta$, $\hat{\mathbf{q}}_3 = \cos\alpha\sin\beta$ so that integration of the scalar term $\mathcal{A}$ over β can be performed directly.

In addition, we are only concerned by the imaginary part of $\Sigma^{(2)}$. This appears through the calculation of $\int d\mathbf{q}\mathcal{A} f[k\mathsf{R}_{31} - q\hat{\mathbf{q}}_1]$ and (with $a \equiv \sin\alpha$ and integrating over β)

$$\mathrm{Im}\left[\int d\mathbf{q}\mathcal{A} f(k\mathsf{R}_{31} - q\hat{\mathbf{q}}_1)\right] = \frac{\pi\omega^3}{2\rho c_T^5}\int_{-1}^{1} da\left\{(1 - 3a^2 + 4a^4) f(k_T a - k\mathsf{R}_{31}) + \frac{4}{\gamma^5}a^2(1 - a^2) f(k_L a - k\mathsf{R}_{31})\right\}. \tag{A8}$$

The remaining integral over the Euler angle θ is performed over $\mathbf{V}^t\mathbf{V}$ with $V_1 = -\sin\theta\cos\xi\sin\varphi + \cos 2\varphi\cos\theta\sin\xi$, $V_2 = \cos\theta\cos\xi\sin\varphi + \cos 2\varphi\sin\theta\sin\xi$, $V_3 = \sin 2\varphi\sin\xi$. This integration is sufficient to show that $\Sigma^{(2)}$ is diagonal with $\Sigma_T^{(2)} = \Sigma_{11}^{(2)} = \Sigma_{22}^{(2)}, \Sigma_L^{(2)} = \Sigma_{33}^{(2)}$ and we get (with $u \equiv \sin\varphi$)

$$\Sigma_T^{(2)} = \rho c_T^2 k^2 F_{2T}(k,\omega), \qquad \Sigma_L^{(2)} = \rho c_T^2 k^2 F_{2L}(k,\omega), \tag{A9}$$

$$F_{2T} \equiv \frac{i}{2\pi^7}\left(\frac{D}{\bar{h}}\right)^2 nL^3x^3\int_{-1}^{1} du[\cos^2\xi u^2 + \sin^2\xi(1 - 2u^2)^2] \times \int_{-1}^{1} da\, h_x(a,u)\int_0^{2\pi} d\xi g_x(\xi,u),$$

$$F_{2L} \equiv \frac{4i}{\pi^7}\left(\frac{D}{\bar{h}}\right)^2 nL^3x^3\int_{-1}^{1} duu^2(1 - u^2) \times \int_{-1}^{1} dah_x(a,u)\int_0^{2\pi} d\xi \sin^2\xi g_x(\xi,u), \tag{A10}$$

$$h_x(a,u) \equiv (1 - 3a^2 + 4a^4) f[(k_T a - ku)D] + \frac{4}{\gamma^5}a^2(1 - a^2) f[(k_L a - ku)D],$$

$$g_x(\xi,u) \equiv \underline{R}[S(\sqrt{1 - u^2}\cos\xi v, x)]^2.$$

APPENDIX B: REMARK ON THE NUMERICAL INTEGRATION OF THE ATTENUATION

The numerical integration of the attenuations in Eq. (2.14) is fairly simple. Functions $f_{1T,1L}$ involve a single integral easy to perform with a Runge-Kutta scheme with adaptative step size. For f_{2L} (respectively, f_{2T}), the integral is of the form

$$\int_{-1}^{1} duu^2(1 - u^2)\int_{-1}^{1} dah(a,u)\int_0^{2\pi} d\xi g(\xi,u), \tag{B1}$$

and to compute it, we first choose a discretization for the u variable, and then, for each u value, we solve independently

$$\text{find } G_u(2\pi) = \int_0^{2\pi} d\xi g(\xi,u) \text{ by solving the ODE } \frac{dG_u(\xi)}{d\xi} = g(\xi,u), \text{ with } G_u(0) = 0,$$

$$\text{find } H_u(1) = \int_{-1}^{1} dah(a,u) \text{ by solving the ODE } \frac{dH_u(a)}{da} = h(\xi,u), \text{ with } H_u(-1) = 0. \tag{B2}$$

These ordinary differential equation (ODEs) are solved using a classical Runge-Kutta scheme with adaptative step size. The final integral over u is finally performed using the trapezoidal rule.

APPENDIX C: ATTENUATION DUE TO THE FLUCTUATIONS OF THE ELASTIC CONSTANTS

We give here very briefly the main steps in the derivation of the attenuation due to the fluctuations of the elastic constants $c_{ijkl}(\mathbf{x})$ from grain to grain. This is just in order to get the order of magnitude of this effect. A wave propagating in a medium with elastic constants that are space dependent is a solution of

$$\rho\frac{\partial^2}{\partial t^2}v_i(\mathbf{x},t) - \frac{\partial}{\partial x_j}\left(c_{ijkl}(\mathbf{x})\frac{\partial}{\partial x_l}\right)v_k(\mathbf{x},t) = 0. \tag{C1}$$

Writing $c_{ijkl}(\mathbf{x}) = \langle c_{ijkl}\rangle + \delta c_{ijkl}(\mathbf{x})$, where the mean has to be defined, the effect due to this spatial dependence can be encapsulated in a potential $V^T(\mathbf{x})$,

$$\rho\frac{\partial^2}{\partial t^2}v_i(\mathbf{x},t) - \frac{\partial^2}{\partial x_j\,\partial x_l}\langle c_{ijkl}\rangle v_k(\mathbf{x},t) = V_{ik}^T(\mathbf{x})v_k(\mathbf{x},t), \qquad V_{ik}^T(\mathbf{x}) \equiv -\frac{\partial}{\partial x_j}\left(\delta c_{ijkl}(\mathbf{x})\frac{\partial}{\partial x_l}\,.\right). \tag{C2}$$

Writing Eq. (C2) in terms of a potential V^T allows the application of the multiple scattering formalism to solve the Dyson equation.

Most of the literature considers that the difference in elasticity occurs because the grains are not uniformly oriented. Thus the mean $\langle c_{ijkl}\rangle$ is taken over all possible orientations. The elastic constants of a grain with arbitrary orientation can be expressed in terms of the single crystal constants c^0_{ijkl} through $c_{ijkl}=R_{ai}R_{bj}R_{ck}R_{dl}c^0_{ijkl}$. This allows one to derive $\langle c_{ijkl}\rangle$, related to c^0_{ijkl} and to a coefficient η that measures the anisotropy of the single crystal. For example, for cubic symmetry, one has $c^0_{iiii}=c_{11}, c^0_{iijj}=c_{12}$, $c^0_{ijij}=c_{44}$ (and zero otherwise) and one gets for an untextured polycrystal (that is, all possible orientations have equal probability), $\langle c_{iiii}\rangle=c_{11}-2\eta/5$, $\langle c_{ijij}\rangle=c_{44}-\eta/5$, with $\eta=c_{11}-c_{12}-2c_{44}$. Within a single grain, the elastic constants c_{ijkl} are indeed constants, and the spatial dependence in $c_{ijkl}(\mathbf{x})$ indicates that the wave travels through different grains.

Assuming small scattering strength, the mass operator can be expanded as in Eq. (2.7). The first-order expansion being proportional to $\langle \delta c_{ijkl}\rangle$, that is zero by definition. The second order is the lowest nonvanishing contribution and it takes the form $\Sigma_2=\langle V^T G^0 V^T\rangle$. In Fourier space, $\Sigma^{(2)}$ can be calculated as follows:

$$\Sigma^{(2)}_{ij}(\mathbf{k}) = \frac{1}{\mathcal{V}}\int d\mathbf{C}d\mathbf{x}d\mathbf{x}' e^{-i\mathbf{kx}}V^T_{ik}(\mathbf{x})G^0_{km}(\mathbf{x}-\mathbf{x}')V^T_{mj}(\mathbf{x}')e^{i\mathbf{kx}'}$$
$$= \frac{1}{\mathcal{V}}\int d\mathbf{C}d\mathbf{x}d\mathbf{x}' e^{-i\mathbf{kx}}\frac{\partial}{\partial x_n}\left(\delta c_{inkl}(\mathbf{x})\frac{\partial}{\partial x_l}G^0_{km}(\mathbf{x}-\mathbf{x}')\right)$$
$$\times\frac{\partial}{\partial x'_p}\left(\delta c_{mpjq}(\mathbf{x}')\frac{\partial}{\partial x'_q}e^{i\mathbf{kx}'}\right). \quad \text{(C3)}$$

To illustrate the calculation, consider the following term (others involve similar calculations):

$$\Sigma^{(2)}_{ij}(\mathbf{k}) = \frac{1}{\mathcal{V}}\int d\mathbf{C}d\mathbf{x}d\mathbf{x}' e^{-i\mathbf{kx}}\delta c_{inkl}(\mathbf{x})\delta c_{mpjq}(\mathbf{x}')$$
$$\times\frac{\partial^2}{\partial x_l\,\partial x_n}G^0_{km}(\mathbf{x}-\mathbf{x}')\frac{\partial}{\partial x'_q\,\partial x'_p}e^{i\mathbf{kx}'}. \quad \text{(C4)}$$

We use $G^0(\mathbf{x})=\int d\mathbf{q}G^0(\mathbf{q})e^{i\mathbf{qx}}/(2\pi)^3$ to get

$$\Sigma^{(2)}(\mathbf{k}) = \frac{1}{\mathcal{V}(2\pi)^3}k^2\int d\mathbf{q}\; q^2G^0(q)\int d\mathbf{x}d\mathbf{x}' e^{-i(\mathbf{k}-\mathbf{q})(\mathbf{x}-\mathbf{x}')}$$
$$\times\int d\mathbf{C}\,\delta c_{ijkl}(\mathbf{x})\delta c_{mnpq}(\mathbf{x}'), \quad \text{(C5)}$$

where we have omitted the indices for simplicity. To evaluate the integral, we now need the geometric correlation function $W(r)$ in the two point average [$W(r)$ is implicitly included in $d\mathbf{C}$]: $W(r)$ represents the probability that two points separated by r are in the same grain. Usually, it is taken as $W(r)=e^{-r/d}$, with d the grain size. For simplicity again, we use instead $W(r)=d^3\delta(r)$. In this way we get

$$\Sigma^{(2)}(\mathbf{k}) \sim \frac{d^3}{(2\pi)^3}k^2\int d\mathbf{q}q^2G^0(q)\langle\delta c_{inkl}\delta c_{mpjq}\rangle$$
$$\sim \frac{id^3}{4\pi\mu}k^2k_L^3\langle\delta c_{inkl}\delta c_{mpjq}\rangle, \quad \text{(C6)}$$

where the angular brackets denote an average over possible orientations. We have considered the longitudinal wave using $G^0(q)=1/(\mu(q^2-k_L^2))$ and focused on the imaginary part of $\Sigma^{(2)}$ only to get the attenuation. With $\langle\delta c_{inkl}\delta c_{mpjq}\rangle=\langle c_{inkl}c_{mpjq}\rangle-\langle c_{inkl}\rangle\langle c_{mpjq}\rangle$, it is possible to end the calculation. Again, the result depends on the symmetry of the single crystal and on the presence or absence of texture. In the simple case of polycrystals of cubic symmetry, one gets $\langle c_{inkl}c_{mpjq}\rangle-\langle c_{inkl}\rangle\langle c_{mpjq}\rangle\propto\eta^2$ so that, for the longitudinal wave,

$$\Sigma^{(2)}(k_L) = \frac{id^3}{4\pi}k_L^5\frac{\eta^2}{\mu}. \quad \text{(C7)}$$

The modified Green function $\langle G\rangle^{-1}=\mu(k^2-K_L^2)$, where K_L is the modified wave number whose imaginary part gives the attenuation coefficient. From $\langle G\rangle^{-1}=G^{0-1}-\Sigma$ with K_L expected to be close to k_L, we get, using $K_L\simeq k_L+\Sigma/(2\mu kL)$,

$$\alpha d \sim \frac{1}{8\pi}\left(\frac{\omega d}{c}\right)^4\left(\frac{\eta}{\mu}\right)^2. \quad \text{(C8)}$$

What happens if both effects, the effect of the change of elastic constants because of the anisotropy and the effect of the dislocations, are considered together?

It is sufficient to sum the potentials $V^T=V^{\text{disloc}}+V^{\text{anisot}}$ to answer. At first order, the linearity implies $\Sigma^{(1)}$ is simply the sum of both effects, and we recover the effect of the dislocation only. At second order, cross terms appear because the nonlinearity in the potential. However, we have in that case

$$\Sigma^{(2)} = \langle V^T G^0 V^T\rangle - \langle V^T\rangle G^0\langle V^T\rangle = \Sigma^{(2),\text{disloc}} + \Sigma^{(2),\text{anisot}}$$
$$+\langle V^{\text{disloc}}G^0V^{\text{anisot}}\rangle + \langle V^{\text{anisot}}G^0V^{\text{disloc}}\rangle$$
$$-\langle V^{\text{disloc}}\rangle G^0\langle V^{\text{anisot}}\rangle - \langle V^{\text{anisot}}\rangle. \quad \text{(C9)}$$

The cross terms involving coupled effects of the dislocations and of the change in elastic effects vanish: this is because the parameters for the average for the anisotropy, typically the orientation of the crystal axis in a grain, are different from the parameters describing the parameters for the average for the grain boundaries: typically the number of dislocations per grain boundary. Thus, we get $\langle V^{\text{disloc}}G^0V^{\text{anisot}}\rangle=\langle V^{\text{disloc}}\rangle G^0\langle V^{\text{anisot}}\rangle$ and simply

$$\Sigma^{(2)} = \Sigma^{(2),\text{disloc}} + \Sigma^{(2),\text{anisot}}. \quad \text{(C10)}$$

[1] W. P. Mason and H. J. McSkimin, "Attenuation and scattering of high frequency sound waves in metals and glasses," J. Acoust. Soc. Am. **19**, 464–473 (1947).
[2] A. B. Bathia, "Scattering of high-frequency sound waves in polycrystalline materials," J. Acoust. Soc. Am. **31**, 16–23 (1959).
[3] E. P. Papadakis, "Grain-size distribution in metals and its influence on ultrasonic attenuation measurements," J. Acoust. Soc. Am. **33**, 1616–1621 (1961).
[4] E. P. Papadakis, "Ultrasonic attenuation caused by scattering in polycrystalline metals," J. Acoust. Soc. Am. **37**, 703–710 (1965).
[5] F. E. Stanke and G. S. Kino, "A unified theory for elastic wave propagation in polycrystalline materials," J. Acoust. Soc. Am. **75**, 665–681 (1984).
[6] S. Hirsekorn, "The scattering of ultrasonic waves by polycrystals," J. Acoust. Soc. Am. **72**, 1021–1031 (1982).
[7] S. Hirsekorn, "The scattering of ultrasonic waves in polycrystalline materials with texture," J. Acoust. Soc. Am. **77**, 832–843 (1985).
[8] S. I. Rokhlin, T. K. Bolland, and L. Adler, "High-frequency ultrasonic wave propagation in polycrystalline materials," J. Acoust. Soc. Am. **91**, 151–165 (1992).

[9]S. Ahmed and R. B. Thompson, "Propagation of elastic waves in equiaxed stainless-steel polycrystal with alignes [001] axes," J. Acoust. Soc. Am. **99**, 2086–2096 (1995).
[10]J. A. Turner, "Elastic wave propagation and scattering in heterogeneous media: Textured polycrystalline materials," J. Acoust. Soc. Am. **106**, 541–552 (1999).
[11]B. R. Thompson, "Elastic-wave propagation in random polycrystals: Fundamentals and application to nondestructive evaluation," in Imaging of Complex Media with Acoustic and Seismic Waves, edited by M. Fink *et al.* [Top. Appl. Phys. **84**, 233–256 (2002)].
[12]X.-G. Zhang, W. A. Simpson, Jr., and J. M. Vitek, "Ultrasonic attenuation due to grain boundary scattering in copper and copper-aluminum," J. Acoust. Soc. Am. **116**, 109–116 (2004).
[13]D. H. Hurley, O. B. Wright, O. Matsuda, T. Suzuki, S. Tamura, and Y. Sugawara, "Time-resolved surface acoustic wave propagation across a single grain boundary," Phys. Rev. B **73**, 125403 (2006).
[14]A. Maurel, V. Pagneux, D. Boyer, and F. Lund, "Propagation of elastic waves through polycrystals: The effects of scattering from dislocation arrays," Proc. R. Soc. London, Ser. A **462**, 2607–2623 (2006).
[15]A. Maurel, V. Pagneux, F. Barra, and F. Lund, "Wave propagation through a random array of pinned dislocations: Velocity change and attenuation in a generalized Granato and Lücke theory," Phys. Rev. B **72**, 174111 (2005).
[16]J. M. Burgers, "Geometrical considerations concerning the structural irregularities to be assumed in a crystal," Proc. Phys. Soc. London **52**, 23–33 (1940).
[17]W. L. Bragg, "The structure of a cold-worked metal," Proc. Phys. Soc. London **52**, 105–109 (1940).
[18]W. Shockley and W. T. Read, "Quantitative predictions from dislocation models of crystal grain boundaries," Phys. Rev. **75**, 692 (1949).
[19]W. T. Read and W. Shockley, "Dislocation models of crystal grain boundaries," Phys. Rev. **78**, 275–289 (1950).
[20]F. C. Frank, in *Proceedings of the Symposium on the Plastic Deformation of Crystalline Solids* (Office of Naval Research, Pittsburgh, PA, 1950), p. 150 [as cited by W. T. Read in *Dislocations in Crystals* (McGraw-Hill, New York, 1953)].
[21]R. S. Wagner and B. Chalmers, "Grain boundaries in germanium," J. Appl. Phys. **31**, 581–587 (1960).
[22]A. R. Patel and C. C. Desai, "Low angle tilt boundaries in synthetic calcium fluoride," Br. J. Appl. Phys. **16**, 1297–1301 (1965).
[23]W. Bollman, *Crystal Defects and Crystalline Interfaces* (Springer, Berlin, 1970).
[24]W. Bollmann, "Basic concepts of O-lattice theory," Surf. Sci. **31**, 1–31 (1972).
[25]K. Sadanada and M. J. Marcinkowski, "Extension of the unified theory of grain boundaries. I. Structure of the boundaries," J. Appl. Phys. **45**, 1521–1532 (1974).
[26]D. Romeu, L. Bertrán del Rio, J. L. Aragón, and A. Gómez, "Detailed atomistic structure of arbitrary fcc [100] twist grain boundaries," Phys. Rev. B **59**, 5134–5141 (1999).
[27]D. M. Duffy, "Grain boundaries in ionic crystals," J. Phys. C **19**, 4393–4412 (1986).
[28]H. Jang and D. Farkas, "Determination of grain boundary geometry using TEM," J. Mater. Res. **7**, 1707–1717 (1992).
[29]L. Sagalowicz and W. A. T. Clark, "A theoretical and experimental study of non perfect grain boundary dislocations," Interface Sci. **4**, 29–45 (1996).
[30]L. Fionova, T. Watanabe, and Yulii Lisovski, "A prospect of grain boundary engineering for electronic properties in polycrystalline materials," ISIJ Int. **36**, 613–623 (1996).
[31]D. A. Hugues, Q. Liu, D. C. Chrzan, and N. Hansen, "Scaling of microstructural paramaters: Misorientations of deformation induced boundaries," Acta Mater. **45**, 105–112 (1997).
[32]X. Pan and J. G. Zheng, "Microstructural of crystal defects in the nanocrystalline tin dioxide thin film," Mater. Res. Soc. Symp. Proc. **472**, 87–92 (1997).
[33]J. Gubicza, G. Ribárik, G. R. Goren-Muginstein, A. R. Rosen, and T. Ungár, "The density and the character of dislocations in cubic and hexagonal polycrystals determined by X-ray diffraction," Mater. Sci. Eng., A **309–310**, 60–63 (2001).
[34]R. Kobayashi, J. A. Warren, and W. C. Carter, "A continuum model of grain boundaries," Physica D **140**, 141–150 (2000).
[35]E. Z. Meilikhov, "Modified dislocation model of intergrain tilt boundaries in HTSC," Physica C **271**, 277–285 (1996).
[36]A. Maurel, J.-F. Mercier, and F. Lund, "Scattering of an elastic wave by a single dislocation," J. Acoust. Soc. Am. **115**, 2773–2780 (2004).
[37]A. Maurel, V. Pagneux, F. Barra, and F. Lund, "Interaction between an elastic wave and a single pinned dislocation," Phys. Rev. B **72**, 174110 (2005).
[38]F. Lund, "Response of a stringlike dislocation loop to an external stress," J. Mater. Res. **3**, 280–297 (1988).
[39]M. O. Peach and J. S. Koehler, "The force exerted on dislocations and the stress fields produced by them," Phys. Rev. **80**, 436–439 (1950).
[40]J. S. Koehler, in *Imperfections in Nearly Perfect Crystals*, edited by W. Schockley *et al.* (Wiley, New York, 1952).
[41]T. Mura, "Continuous distribution of moving dislocations," Philos. Mag. **8**, 843–857 (1963).
[42]P. Sheng, *Scattering and Localization of Classical Waves in Random Media* (World Scientific, Singapore, 1990).
[43]P. Sheng, *Introduction to Wave Scattering, Localization, and Mesoscopic Phenomena* (Academic, New York, 1995).
[44]B. Velicky, "Sound in granular matter," lecture notes, http://cel.archives-ouvertes.fr/docs/00/09/29/42/PDF/velicky.pdf, last accessed 5 December 2006.
[45]P. Lacombe, *Report of Conference on Strength Solids* (The Physical Society of London, London, 1948).
[46]T. Suzuki, M. Aoki, and A. Ikushima, "Acoustic attenuation studies of frictional force on fast moving dislocation," Acta Metall. **12**, 1231–1240 (1964).
[47]W. P. Mason and A. Rosenberg, "Phonon and electron drag coefficients in single-crystal aluminum," Phys. Rev. **151**, 434–441 (1966).
[48]T. Ninomiya, "Frictional force acting on a dislocation-fluttering mechanism," J. Phys. Soc. Jpn. **36**, 399–405 (1974).
[49]D. W. Krautkopf, "Ultrasonic scattering and attenuation in polycrystalline copper and α-Brass," J. Acoust. Soc. Am. **32**, 824–835 (1960).
[50]A. V. Granato and K. Lücke, in *Physical Acoustics*, edited by W. P. Mason (Academic, New York, 1966), Vol. **4A**.
[51]A. V. Granato and K. Lücke, "Theory of mechanical damping due to dislocations," J. Appl. Phys. **27**, 583–593 (1956).
[52]A. V. Granato and K. Lücke, "Application of dislocation theory to internal friction phenomena at high frequencies," J. Appl. Phys. **27**, 789–805 (1956).
[53]K. Lücke and A. V. Granato, "Simplified theory of dislocation damping including point-defect drag. I. Theory of drag by equidistant point defects," Phys. Rev. B **24**, 6991–7006 (1981).
[54]A. V. Granato and K. Lücke, "Simplified theory of dislocation damping including point-defect drag. II. Superposition of continuous and pinning-point-drag effects," Phys. Rev. B **24**, 7007–7017 (1981).
[55]A. Hikata, R. Truel, A. Granato, B. Chick, and K. Lücke, "Sensitivity of ultrasonic attenuation and velocity changes to plastic deformation and recovery in aluminum," J. Appl. Phys. **27**, 396–404 (1956).
[56]H. Ogi, M. Hirao, and K. Minoura, "Noncontact measurement of ultrasonic attenuation during rotating fatigue test of steel," J. Appl. Phys. **81**, 3677–3684 (1997).
[57]H. Ogi, H. M. Ledbetter, S. Kim, and M. Hirao, "Contactless mode-selective resonance ultrasound spectroscopy: Electromagnetic acoustic resonance," J. Acoust. Soc. Am. **106**, 660–665 (1999).
[58]H. Ogi, A. Tsujimoto, M. Hirao, and H. Ledbetter, "Stress-dependent recovery of point defects in deformed aluminum: An acoustic damping study," Acta Mater. **47**, 3745–3751 (1999).
[59]M. Hirao, H. Ogi, N. Suzuki, and T. Ohtani, "Ultrasonic attenuation peak during fatigue of polycrystalline copper," Acta Mater. **48**, 517–524 (2000).
[60]T. Ohtani, H. Ogi, and M. Hirao, "Acoustic damping characterization and microstucture evolution in nickel-based superalloy during creep," Int. J. Solids Struct. **42**, 2911–2928 (2005).
[61]M. W. Barsoum, M. Radovic, T. Zhen, P. Finkel, and S. R. Kalidindi, "Dynamic elastic hysteretic solids and dislocations," Phys. Rev. Lett. **94**, 085501 (2005).